Analysis of a Method to Estimate Chlorophyll-*a* Concentration from Irradiance Measurements at Varying Depths

JASMINE S. NAHORNIAK, MARK R. ABBOTT, RICARDO M. LETELIER, AND W. SCOTT PEGAU

College of Oceanic and Atmospheric Sciences, Oregon State University, Corvallis, Oregon

(Manuscript received 18 July 2000, in final form 20 June 2001)

ABSTRACT

A model to estimate chlorophyll-*a* concentration and yellow substance absorption at 440 nm from irradiance measurements made at varying depths is examined. The derivation of the model, requiring irradiance measurements at three wavebands, is presented and tested on data collected in oligotrophic (with low chlorophyll concentrations) waters and in coastal waters (with both high and low chlorophyll concentrations). The results indicate excellent quantitative agreement with chlorophyll-*a* concentration and yellow substance absorption measurements. A sensitivity analysis of the model shows it to be highly sensitive to pressure sensor precision, the accuracy of the value used for the mean cosine of the downwelling radiance distribution, and the irradiance sensor measurement error. However, provided that these factors are taken into account, accurate estimates of chlorophyll-*a* concentrations in case I (phytoplankton-dominated) waters using a single (or multiple) irradiance sensor with three wavebands can be derived. This model can be applied to irradiance data from a variety of deployment methods including profilers, bottom-tethered moorings, subsurface drifters, and towed platforms.

1. Introduction

Spectral radiometric measurements are commonly used to estimate chlorophyll-*a* concentration (C) as a proxy for phytoplankton biomass. The algorithms used stem from a study done by Clarke et al. (1970) over three decades ago. They showed the existence of a relationship between chlorophyll concentration at the sea surface and the spectral shape of irradiance reflectance. Since Clarke's original work, numerous empirical models have been developed that utilize optical data (irradiances, radiances, and/or reflectances) in a number of wavelength combinations to estimate C. This principle has been extended to include the estimation of additional parameters such as the concentration of yellow substance (color dissolved organic matter) (e.g., Carder et al. 1991). By providing the means to perform continuous monitoring of these parameters in space and time using satellite and in situ data, such algorithms are powerful tools in the study of water column dynamics on both global and regional scales.

To apply these algorithms throughout the water column, the effect of spectral changes in the light field caused by changes in depth must be considered. Even in homogeneous waters the spectral shape of the downwelling light varies with depth. If measurements are made at a constant depth, this effect can be accounted for by calibrating the spectral irradiance measurements to in situ measurements of C at the same depth (e.g., Smith et al. 1991). For measurements made at varying depths (such as measurements made using profilers, autonomous underwater vehicles, and bottom-tethered moorings that can tilt with the currents), such calibrations are not sufficient to derive accurate estimates of C.

One method commonly used to estimate C from profiles of downwelling irradiance is by calculating the downwelling diffuse attenuation coefficient (K_d), from which C can be estimated using an empirical relationship (Morel 1988; Bricaud et al. 1998). To remove fluctuations in the calculated K_d values caused by variations in the magnitude of downwelling irradiance incident at the sea surface, simultaneous measurements of downwelling irradiance at the sea surface are made. Hence, this method has the disadvantage that two detectors are required.

Recently, a model to retrieve C from sensors with varying depths was presented (Bartlett et al. 1998a). This method has the advantage that it requires measurements made with only one detector. The present study investigates the accuracy and precision of the input parameters required to retrieve accurate estimates of C. We present the application of this model to data from profiling optical instruments in different water types. Furthermore, we discuss the application of this model to long-term deployments, such as bottom-tethered moorings.

Corresponding author address: Jasmine S. Nahorniak, 104 Ocean Admin. Bldg., COAS, Oregon State University, Corvallis, OR 97331. E-mail: jasmine@coas.oregonstate.edu

TABLE 1. List of symbols.

$A(\lambda_i, \lambda_j)$, A_i	Spectral constant in the δK_{ji} equation (m^{-1})
$a(\lambda)$	Total absorption coefficient (m^{-1})
$a_p(\lambda)$	Absorption coefficient for particles (m^{-1})
$a^*_{ph}(\lambda)$	Normalized specific absorption coefficient for phytoplankton (ND)*
$a_{ph}(\lambda)$	Absorption coefficient for phytoplankton (m^{-1})
$a_w(\lambda)$	Absorption coefficient for pure seawater (m^{-1})
$a_y(\lambda)$	Absorption coefficient for yellow substance (m^{-1})
$B(\lambda_i, \lambda_j)$, B_i	Spectral constant in the δK_{ji} equation (m^{-1})
$b_b(\lambda)$	Total backscattering coefficient (m^{-1})
$\tilde{b}_{bp}$	Proportion of backscattering to total scattering by particles (ND)
$b_{bph}(\lambda)$	Backscattering coefficient for phytoplankton (m^{-1})
$b_{bw}(\lambda)$	Backscattering coefficient for pure seawater (m^{-1})
$b_w(\lambda)$	Scattering coefficient for pure seawater (m^{-1})
$C(z)$	Chlorophyll-*a* concentration (mg m^{-3})
$D(\lambda_i, \lambda_j)$, D_i	Spectral constant in the δK_{ji} equation (ND)
$E_d(\lambda, z)$	Downwelling irradiance (μW cm^{-2} nm^{-1})
$K_d(\lambda, z)$	Downwelling diffuse attenuation coefficient for irradiance (m^{-1})
z	Depth (m)
z'	Apparent depth of the sensor (m)
z_{mn}	Average of z_m and z_n (m)
$\delta K_{ji}(z)$	Diffuse attenuation coefficient difference $K_d(\lambda_j, z) - K_d(\lambda_i, z)$ (m^{-1})
γ	$-D_1/D_2$ (ND)
λ	Wavelength (nm)
μ_d	Mean cosine for the downwelling light field (ND)
θ	Angle of the sensor from the vertical (degrees)

* ND represents a nondimensional parameter.

2. Model description

The model is an extension to an analytic model presented by Waters (1989). It is based on the following relationship for the variation of irradiance with depth:

$$E_d(\lambda, z_n) = E_d(\lambda, z_m) \exp[-K_d(\lambda, z_{mn})(z_n - z_m)], \quad (1)$$

where $E_d(\lambda, z)$ is the downwelling irradiance at wavelength λ and depth z, and $K_d(\lambda, z_{mn})$ is the average downwelling irradiance attenuation coefficient between depths z_m and z_n. This relationship assumes that $K_d(\lambda, z)$ does not vary substantially between the depths z_m and z_n. A list of symbols can be found in Table 1.

The model derivation involves calculating irradiance ratios $E_d(\lambda_i, z_n)/E_d(\lambda_j, z_n)$ from (1):

$$\frac{E_d(\lambda_i, z_n)}{E_d(\lambda_j, z_n)} = \frac{E_d(\lambda_i, z_m)}{E_d(\lambda_j, z_m)} \exp[\delta K_{ji}(z_{mn})(z_n - z_m)], \quad (2)$$

where

$$\delta K_{ji}(z) = K_d(\lambda_j, z) - K_d(\lambda_i, z). \quad (3)$$

Rearranging (2) yields

$$\delta K_{ji}(z_{mn}) = \ln\left[\frac{E_d(\lambda_i, z_n)}{E_d(\lambda_j, z_n)} \frac{E_d(\lambda_j, z_m)}{E_d(\lambda_i, z_m)}\right](z_n - z_m)^{-1}. \quad (4)$$

Hence, δK_{ji} can be estimated either from measurements of $E_d(\lambda, z)$ and depth directly [Eq. (4)] or from calculated diffuse attenuation coefficient values [Eq. (3)]. The advantage of this method is that it is based solely on variations in irradiance ratios (which describe the spectral shape of the downwelling light field), rather than on fluctuations in the magnitude of the downwelling irradiance. Changes in cloud cover between measurements can cause strong fluctuations in the magnitude of irradiance, but relatively small (although nonnegligible) fluctuations in the spectral shape (Bartlett et al. 1998b).

In the absence of scattering, the downwelling diffuse attenuation coefficient is given by

$$K_d(\lambda) = a(\lambda)/\mu_d, \quad (5)$$

where $a(\lambda)$ is the total absorption coefficient and μ_d is the mean cosine of the downwelling light field. The depth dependence has been dropped for brevity. The mean cosine is assumed to be independent of wavelength and depth over the depth range of interest; the consequence of this assumption is examined in section 3a. The effect of backscattering is discussed in section 3b.

In phytoplankton-dominated (case I) waters, the absorption coefficient can be expressed in terms of $a_y(440)$ (the absorption coefficient for yellow substance at 440 nm) and C (Prieur and Sathyendranath 1981; Bricaud et al. 1981; Morel 1991) as

$$\begin{aligned} a(\lambda) &= a_w(\lambda) + a_{\text{ph}}(\lambda) + a_y(\lambda) \\ &= a_w(\lambda) + 0.06a^*_{\text{ph}}(\lambda)C^{0.65} \\ &\quad + a_y(440)\exp[-0.014(\lambda - 440)], \end{aligned} \quad (6)$$

where $a_w(\lambda)$, $a_{\text{ph}}(\lambda)$, and $a_y(\lambda)$ are the absorption coefficients for pure seawater, phytoplankton, and yellow substance, respectively, and $a^*_{\text{ph}}(\lambda)$ is the specific absorption coefficient for phytoplankton normalized to the value at 440 nm. The effect of detritus is neglected. Assuming that this relationship is valid in the regions and depths of interest, δK_{ji} can then be calculated as a function of C and $a_y(440)$ using (5) and (3) (see the appendix).

Since δK_{ji} is expressed as a function of two unknowns, two δK_{ji} equations (using different wavelength pairs) can be used to solve for C and $a_y(440)$ (see the appendix). Care must be taken to choose wavelength pairs that best describe the effect of C and $a_y(440)$ on the downwelling irradiance spectrum, while avoiding wavelengths with either very low irradiance values (e.g., long wavelengths) or contributions from other sources (e.g., Raman scattering). For examples of the spectral shape of the downwelling light field for different values of C, see Morel (1988, his Fig. 12). Wavelengths commonly used in remote sensing measurements of ocean color include 412, 443, 490, 511, 555, 670, 683, and 700 nm. The modeled dependencies of δK_{ji} on C and $a_y(440)$ for pairs of the shorter wavelengths (412–555 nm) are shown in Fig. 1 (see also Bartlett et al. 1998a). To solve for C and $a_y(440)$, two δK_{ji}'s must be chosen with trends that intersect. From Fig. 1, the δK_{ji} with a trend that differs the most from the others is $\delta K_{443,412}$ (Fig. 1a). To minimize the number of measurements that must be made, another wavelength pair will be chosen

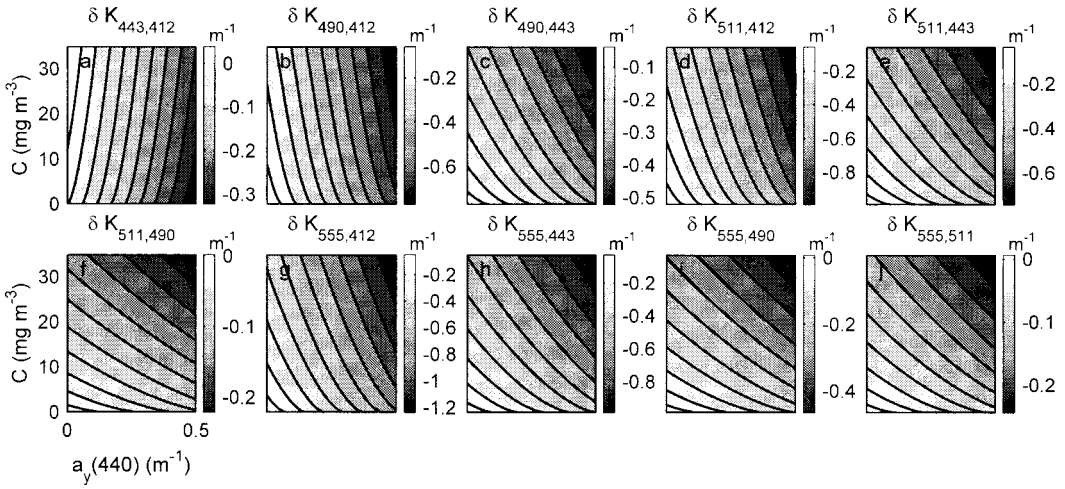

FIG. 1. Modeled dependence of δK_{ji} on C and $a_y(440)$ for different wavelength pairs.

that includes either 412 or 443 nm. Of these two wavelengths, the δK_{ji}'s with trends that intersect $\delta K_{443,412}$ with the largest angle are those that include 443 nm (i.e., Figs. 1c,e,h), and of these δK_{ji}'s the largest angles are made by $\delta K_{555,443}$ and $\delta K_{511,443}$. The set of wavelength pairs (412, 443) and (443, 555) yields (see the appendix and Table 2)

$$C = \left[\frac{\mu_d(\delta K_{443,412} - 0.687\delta K_{555,443}) + 0.0336}{0.0372}\right]^{1.54}, \quad (7)$$

and

$$a_y(440) = \frac{\mu_d \delta K_{443,412} - 0.00251 - 0.00570C^{0.65}}{-0.521}. \quad (8)$$

The wavelength pairs (412, 443) and (443, 511) will be shown to be a more robust set of wavelength pairs for waters with low chlorophyll concentrations. This set of wavelength pairs yields

$$C = \left[\frac{\mu_d(\delta K_{443,412} - 0.885\delta K_{511,443}) + 0.0217}{0.0344}\right]^{1.54}, \quad (9)$$

and

$$a_y(440) = \frac{\mu_d \delta K_{443,412} - 0.00251 - 0.00570C^{0.65}}{-0.521}$$

(as above). (10)

Note that other combinations of wavelengths can be used with similar results.

3. Method assumptions

The accuracy of this method depends on the validity of several assumptions: 1) the empirical relationships and parameter values used are representative of the region and depth being studied, 2) the variation in the spectral shape of the light field at the sea surface is negligible between successive measurements at depths z_m and z_n, and 3) the measurement precision and resolution are adequate.

Using appropriate empirical relationships and parameter values for the region, the effects of the first assumption can be minimized. The effects of the mean cosine accuracy and backscattering are examined below.

The second assumption can be made only if the measurement frequency is high enough such that spectral variations between measurements caused by changes in solar elevation, variations in cloud cover, and wave effects can be assumed to be negligible. Note that at very high frequencies, wave effects may become important near the sea surface (Siegel and Dickey 1988).

The effects of the third assumption can be minimized by utilizing instruments with high precision and resolution. These requirements are examined in section 3c.

a. Sensitivity to the mean cosine

From (9) and (10) it is seen that the model is a function of the mean cosine μ_d. This parameter is a function of water type, depth, the angle and distribution of incident light, and wavelength. For vertically incident light, μ_d takes a value of approximately 0.95 at the sea surface, and decreases to an asymptote of approximately 0.7 at the 1% light level (the actual values for μ_d depend on the water type and wavelength) (Kirk 1994). For light incident at an angle to the sea surface, the surface value for μ_d is decreased, but the asymptote value remains the same. In waters where scattering dominates absorption, μ_d can approach a value of 0.5 at depth. In spite of this range in values for μ_d, it is often represented by a constant.

To assess the effect of an incorrect mean cosine in the model, errors of $\pm 10\%$ are added to a mean cosine value of 0.8 (a typical, midwater column value). Next, $\delta_{ji}K$'s are calculated for these different mean cosines for various values of C and $a_y(440)$ using Eq. (A1) (from

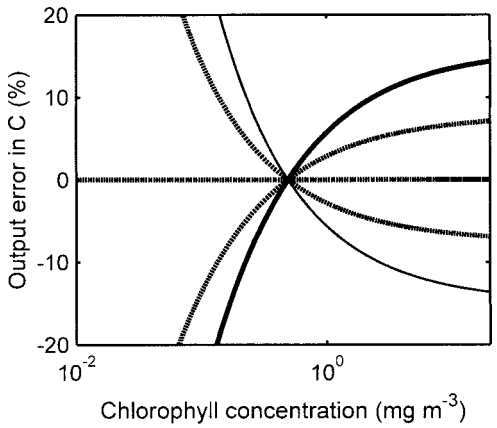

FIG. 2. Modeled percentage error in the estimated C [from Eq. (9)] as a function of the actual C. Different errors were applied to the value of μ_d used to calculate δK_{ji}, from −10% (thin solid curve) to +10% (thick solid curve) of 0.8, whereas a value of 0.8 was used in the model. The wavelength pairs used were (412, 443) and (443, 511), with parameter values from Table 3 and $a_y(440) = 0.1$ m^{-1}. Similar results are obtained using wavelength pairs (412, 443) and (443, 555) and other values of $a_y(440)$ (not shown).

the appendix). Then C is estimated using a constant mean cosine of 0.8 in the model [Eq. (9)]. The percentage errors between the estimated C and actual C are then calculated (Fig. 2).

The model shows a strong dependence on the value of mean cosine used. At chlorophyll-*a* concentrations above 0.5 mg m^{-3}, the output error for C increases with C to an asymptote of approximately the same magnitude as the error in the mean cosine. For a C value of 0.5 mg m^{-3}, the output error in C is negligible regardless of the mean cosine error. At lower values of C, the output error increases with decreasing values of C. The output error for C is independent of the actual value of $a_y(440)$ (not shown). In other words, except for chlorophyll-*a* concentrations below 0.2 mg m^{-3}, the error in the estimated values for C are approximately equal to or less than the error in the input values of μ_d. Ideally, accurate estimates for the mean cosine should be used to derive accurate estimates of C using this method; however, in most applications μ_d is unknown. The results shown here illustrate that, for waters with chlorophyll-*a* concentrations above 0.2 mg m^{-3} (with values of μ_d between 0.72 and 0.88), approximating μ_d by 0.8 causes a maximum error in the estimated C of 13%.

b. The effect of backscattering

The relationship for $K_d(\lambda)$ used in this study neglects the effect of backscattering. To determine the effect of this assumption, two versions of this model were used to estimate C and the results were compared. The first, simpler model neglects scattering [as presented here; see Eq. (5)]. The second, more complex model incorporates backscattering by water and phytoplankton by using a relationship for $K_d(\lambda)$ of the form (Sathyendranath and Platt 1988)

$$K_d(\lambda) = [a(\lambda) + b_b(\lambda)]/\mu_d, \tag{11}$$

where (Gordon and Morel 1983; Sathyendranath et al. 1989)

$$\begin{aligned} b_b(\lambda) &= b_{bw}(\lambda) + b_{b\mathrm{ph}}(\lambda) \\ &= 0.5b_w(\lambda) + \tilde{b}_{bp}0.3(550/\lambda)C^{0.62}, \end{aligned} \tag{12}$$

$b_{bw}(\lambda)$ and $b_{b\mathrm{ph}}(\lambda)$ are the backscattering coefficients for pure seawater and phytoplankton, respectively, $b_w(\lambda)$ is the scattering coefficient for pure seawater, and $\tilde{b}_{bp}$ is the proportion of backscattering to total scattering by particles. By assuming that $\tilde{b}_{bp}$ is independent of C and approximating $C^{0.62}$ by $C^{0.65}$, the model incorporating backscattering can be derived in a similar manner to that presented in the appendix (Bartlett et al. 1998a), yielding

$$C = \left[\frac{\mu_d(\delta K_{443,412} - 0.687\delta K_{555,443}) + 0.0335}{0.0374}\right]^{1.54}, \tag{13}$$

$$a_y(440) = \frac{\mu_d\delta K_{443,412} - 0.00156 - 0.00542C^{0.65}}{-0.521}, \tag{14}$$

for wavelength pairs (412, 443) and (443, 555), where $\tilde{b}_{bp}$ is approximated by 0.01 (Ulloa et al. 1994), and $b_w(\lambda)$ is given by 0.0067, 0.0048, and 0.0019 m^{-1} at 412, 443, and 555 nm, respectively (Morel 1974).

The estimates for C differed between the two models by between 1% (for $C > 0.2$ mg m^{-3}) and 5% (for C values close to 0.01 mg m^{-3}). The estimates for $a_y(440)$ differed by 0.002 m^{-1} (at $C = 0.01$ mg m^{-3}) to 0.006 m^{-1} (at $C = 20$ mg m^{-3}), which is less than the magnitude of $a_w(440)$ (0.00635 m^{-1}; Pope and Fry 1997). The effects of an incorrect mean cosine or poor pressure sensor precision are significantly higher than the effect of neglecting backscattering. Hence, the benefit of incorporating backscattering in the model is minimal.

TABLE 2. Spectral coefficients used to estimate C and a_y (440) in the model [Eqs. (A1), (A5), and (A6)].

	412, 443 nm	443, 511 nm	443, 555 nm	412, 443, 511 nm	412, 443, 555 nm
A (m^{-1})	0.00251	0.0273	0.0525		
B (m^{-1})	0.00570	−0.0324	−0.0458		
D	−0.521	−0.589	−0.759		
γ				−0.885	−0.687

c. Required measurement resolution and precision

The effects of measurement resolution and precision are examined by studying the effects of input errors in δK_{ji} on the estimated C. By inspecting Eq. (A1) (see the appendix) it is seen that errors in δK_{ji} can be rep-

TABLE 3. Spectral values and sources for the parameters used to estimate C and Y.

	412 nm	443 nm	511 nm	555 nm	Source
a_w (m^{-1})	0.00456	0.00707	0.0344	0.0596	Pope and Fry (1997)
a^*_{ph}	0.887	0.982	0.442	0.219	Hoepffner and Sathyendranath (1993)
μ_d	0.8	0.8	0.8	0.8	Kirk (1994)

resented by errors in μ_d. Hence, the results are the same as those shown in Fig. 2.

Possible contributions to error in δK_{ji} can be found by examining its components. From Eq. (4), the contributors to error in the input δK_{ji} are errors in the irradiance measurements at λ_i and λ_j, and the error in the calculated depth difference.

Error in the irradiance measurements is a function of the instrument accuracy, resolution, and precision, as well as the long-term stability of the instrument. To determine the effects of irradiance measurement error, the errors in the estimated values of C were modeled for instrument errors of 0.01 and 1 μW cm^{-2} nm^{-1} (Fig. 3). For this analysis, yellow substance concentrations were set to zero and a mean cosine of 0.8 was used. The effect of the depth difference used was relatively small; it was set to 1 m. Two different water types [C = 0.1 mg m^{-3} (Figs. 3a,c) and C = 10 mg m^{-3} (Figs. 3b,d)] were tested using the wavelength combinations 412, 443, and 511 nm (Figs. 3a,b) and 412, 443, and 555 nm (Figs. 3c,d).

The figures illustrate that as the irradiance approaches the magnitude of the sensor error with increasing depth, the error in the retrieved C increases dramatically. The depth where this occurs is much shallower for high chlorophyll waters than low chlorophyll waters, and much shallower for high instrument errors than low instrument errors. For example, in Fig. 3c, as the depth increases the first wavelength at which the sensor reaches the magnitude of the sensor error is 555 nm (which reaches a sensor error of 0.01 μW cm^{-2} nm^{-1} at 125 m). At this depth, the error in the retrieved value for C is well above 10% (thin solid curve). The depth at which the retrieval error is equal to 5% is about 90 m in this case.

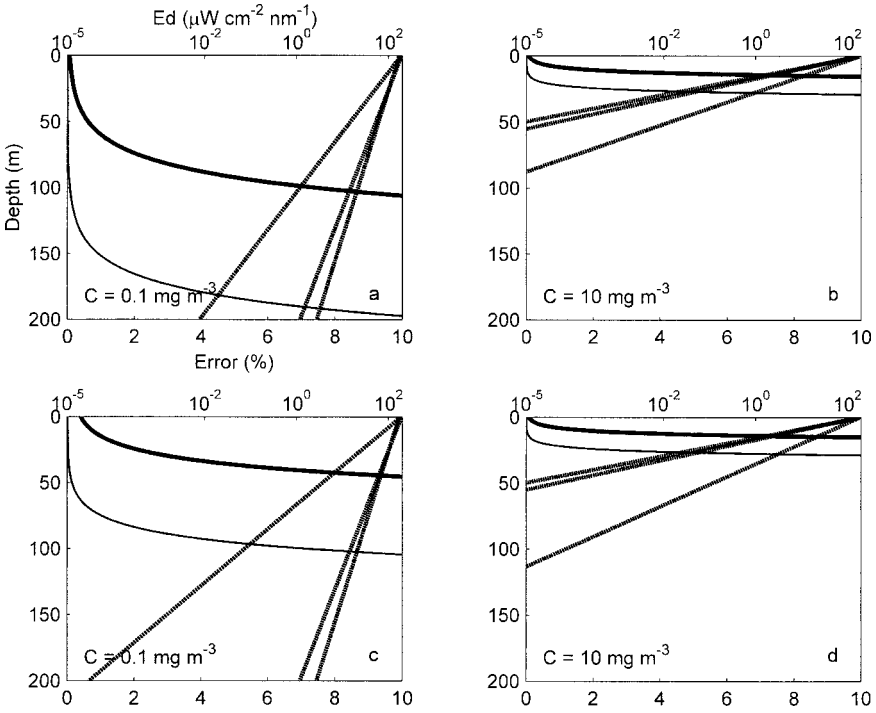

FIG. 3. Modeled relationship between the percentage error in the estimated values for C and the downwelling irradiances as a function of depth. Each panel shows (i) the irradiances as a function of depth for the three wavelengths used (dashed lines), and (ii) the percentage error in the estimated values for C as a function of depth for irradiance sensor errors of 1 μW cm^{-2} nm^{-1} (thick solid curve) and 0.01 μW cm^{-2} nm^{-1} (thin solid curve). (a) Wavelengths 511, 443, and 412 nm from left to right, respectively, and C = 0.1 mg m^{-3}. (b) Wavelengths 443, 412, and 511 nm from top to bottom, respectively, and C = 10 mg m^{-3}. (c) Wavelengths 555, 443, and 412 nm from left to right, respectively, and C = 0.1 mg m^{-3}. (d) Wavelengths 443, 412, and 555 nm from top to bottom, respectively, and C = 10 mg m^{-3}.

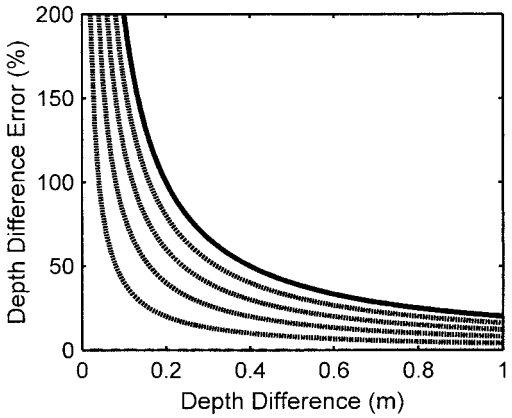

FIG. 4. Modeled percentage error in the depth difference as a function of the depth difference for a range of absolute errors in depth from 0 m (curve along *x* axis) to 0.1 m (solid curve). Each curve represents a 0.02-m increment in the absolute depth error.

For instruments with a higher error of 1 μW cm^{-2} nm^{-1} (thick solid curve), the depth where the retrieval error is 5% is much shallower: 30 m in this case.

Note that the maximum deployment depth depends not only on the instrument error and in situ chlorophyll concentration, but also on the magnitude of the irradiance incident at the sea surface. If less light is available, the irradiance will reach the magnitude of the instrument error at a much shallower depth. Ideally, the deployment depth would be determined based on in situ conditions. Note also that the limiting wavelength varies depending on the water type; in low chlorophyll waters 511 or 555 nm is the limiting wavelength (Figs. 3a,c), whereas 443 nm is the limiting wavelength in high chlorophyll waters (Figs. 3b,d). A general guideline based on this analysis is that instruments should be deployed at depths where the irradiance values at all of the wavelengths to be used are at least 5 times the sensor error.

The pressure sensor precision may also be a significant contributor to the error in the δK_{ji} since it is the error of the depth difference that is important. For example, if measurements are made at 25.1 and 25.3 m (depth difference of 0.2 m), and the precision is 0.1 m (0.4%), then the error in the depth difference is 100%. Hence, the pressure sensor must be highly precise (with high resolution) if small depth differences are used.

The precision of pressure sensors is highly variable. Precision is usually presented as part of the overall accuracy. Examination of several pressure sensors currently available revealed accuracies ranging from 0.01% to 1% of full scale, where the full scales ranged from 10 to 7000 m. The absolute errors of these sensors ranged from 0.001 to 6 m. Resolutions ranged from 0.0001% to 0.25% of full scale (0.00001 to 1.5 m).

Assuming pressure sensors with precisions ranging from 0 to 0.1 m, the effects on the error in the calculated depth difference (δz) are examined for values of δz between 0 and 1 m (Fig. 4). For a precision of 0.02 m (lowest dashed curve), the error in the depth difference varies from 5% to 35% for depth differences of 1 to 0.1 m, respectively. Hence, the precision of the pressure sensor, combined with the desired retrieval accuracy for *C*, defines the depth difference that should be used.

The tilt, roll, and vertical speed of the instrument can also influence the accuracy of the estimated *C*. Tilt and roll can cause variations in the measured spectral shape and μ_d. When the sensor is at an angle from the vertical, the pathlength the light must travel through the water increases, and hence the amount of light attenuation (which is spectrally dependent) also increases. This effect can be accounted for by calculating the apparent depth z' of the sensor based on θ, the angle from the vertical, [$z' = z/\cos(\theta)$], and using this apparent depth when calculating the depth differences. However, as the sensor tilts, its angle with respect to the sun changes, and hence the apparent μ_d also changes (except in diffuse lighting conditions). The vertical speed of the instrument can also affect the estimates of *C* if the pressure cell is affected by the dynamic head. These effects can be minimized by careful instrument deployment and/or by removing measurements with relatively large tilt and roll values and high vertical velocities.

4. Test using profiler data

Our method was tested on data collected from three different sites using different optical profilers. The locations studied were an oligotrophic (low chlorophyll concentration) station near Hawaii, a coastal station off Oregon, and a coastal station in the Gulf of California. These sites were chosen to examine the method's robustness over a range of chlorophyll-*a* concentrations and water types.

Since irradiance measurements during a profile are usually made at high frequency (e.g., 3 Hz), pressure differences between successive measurements can be comparable to the pressure sensor resolution and precision. To increase the accuracy of the calculated depth intervals, the distance between the measurement depths used should be increased. Three possible ways to achieve this are 1) δK_{ji} is calculated using Eq. (3) by calculating the average downwelling diffuse attenuation coefficient over relatively large depth bins (e.g., 4 m), 2) the pairs of data points used are chosen farther apart in time (e.g., every 10 s instead of every 1/3 s), and 3) the pairs of data points are chosen to be as close as possible to a set distance apart (e.g., every 2 m). Since the first method is an average over a bin, it is sensitive to outliers and it tends to smooth the data, thereby removing high-resolution vertical structure. The second method retains more vertical structure information; however, it yields poor results at depths where the instrument is stationary (e.g., at the bottom or top of a profile), and the resulting values of *C* are for depth bins of varying size. The third method overcomes these issues.

At the first location, near Hawaii (station ALOHA;

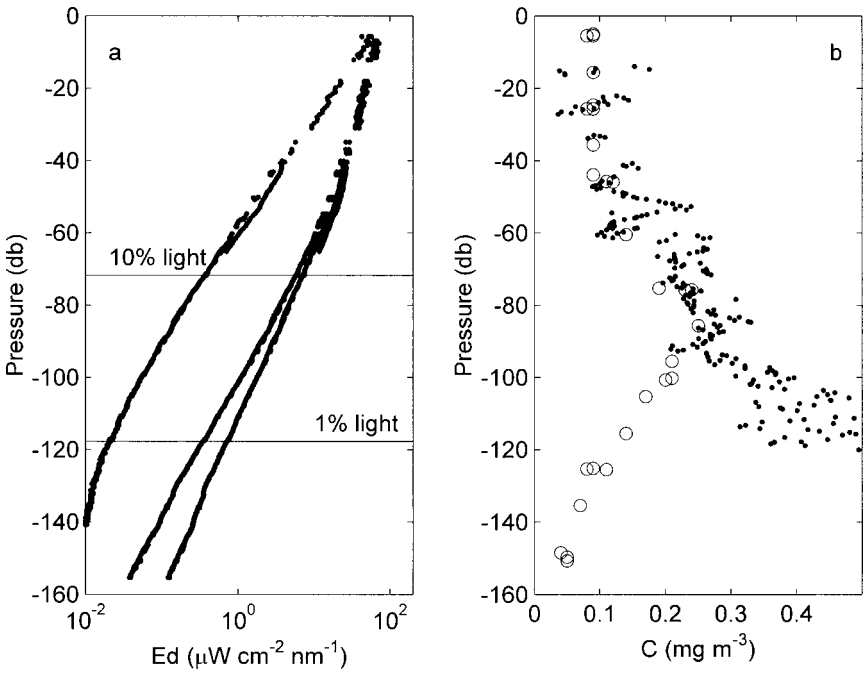

FIG. 5. Downwelling irradiance profiles and estimation of chlorophyll-*a* concentration profiles from PRR measurements and comparison with extracted chlorophyll-*a* measurements made by fluorometric analysis in Hawaiian waters (station ALOHA; 22°45′N, 158°W). (a) Downwelling irradiance profiles at 555, 412, and 443 nm (from left to right) near solar noon on 11 Nov 1998; and (b) estimated chlorophyll-*a* concentration from the PRR measurements (filled circles) compared with extracted chlorophyll-*a* measurements (open circles) from three casts on 10 and 11 Nov 1998. The depths of the 10% and 1% light levels [calculated from $E_d(443)$] are indicated in (a). Measurements from both the downwelling and upwelling portions of the PRR profiles were used. Missing PRR data are a result of tilt and/or roll values greater than 5°. During the PRR measurements, the sky was overcast. The mean cosine was assumed to be 0.8. Bins of 8 m every 0.4 m were used in the calculations.

22°45′N, 158°W), optical profiles were measured using a profiling reflectance radiometer (PRR; Biospherical Instruments Inc.) at six visible wavebands including 412, 443, 511, and 555 nm (Figs. 5a, 6a). The pressure sensor accuracy was 1% of full scale (200 m), that is, 2 m, and the resolution was 0.2 m at depth.

Complementary measurements of extracted chlorophyll-*a* concentration profiles were also made in separate casts (Figs. 5b, 6b). These concentrations were determined using the fluorometric method following extraction in acetone according to Strickland and Parsons (1972) with modifications as reported by Letelier et al. (1996). The values at this location were relatively low (maximum of 0.25 mg m^{-3}). These data are in excellent agreement with chlorophyll-*a* concentrations determined from extracted HPLC (high-pressure liquid chromatography) measurements (not shown) made during one of the three casts; the slope of the linear regression does not differ significantly from one ($r^2 = 0.993$, slope $= 0.94$, intercept $= 0.0017$ mg m^{-3}, $n = 9$, model II geometric mean regression). Hence, the fluorometric chlorophyll-*a* data are representative of the actual chlorophyll-*a* concentrations.

Estimates of C were then made using Eq. (7) with irradiance pairs 8 m apart at 0.4 m intervals, wavelengths 412, 443, and 555 nm, and a mean cosine of 0.8 (Fig. 5b). Pressure differences (as measured by the instrument) were assumed to be equivalent to depth differences. Smaller binning intervals produced noisy profiles for this dataset. This may be a result of the pressure sensor accuracy and resolution as well as the low chlorophyll concentrations (and hence small diffuse attenuation coefficients) involved; spectral changes in the light field are more apparent over larger depth intervals. Measurements with tilt and roll values greater than 5° are not used in this study.

Comparison of the estimated chlorophyll concentration profiles with the extracted chlorophyll measurements shows good agreement near the surface, but poor agreement at depth. This is probably a result of the irradiance at 555 nm approaching the irradiance measurement error at depth (see Fig. 3c). According to the irradiance error analysis outlined in section 3c, accurate retrievals of C can be made at deeper depths in low-chlorophyll waters using 511 nm instead of 555 nm (cf. Figs. 3a,c). Using the measured irradiances at 511 nm in this application improves the results considerably (Fig. 6b). Note that the accuracy for replication of fluo-

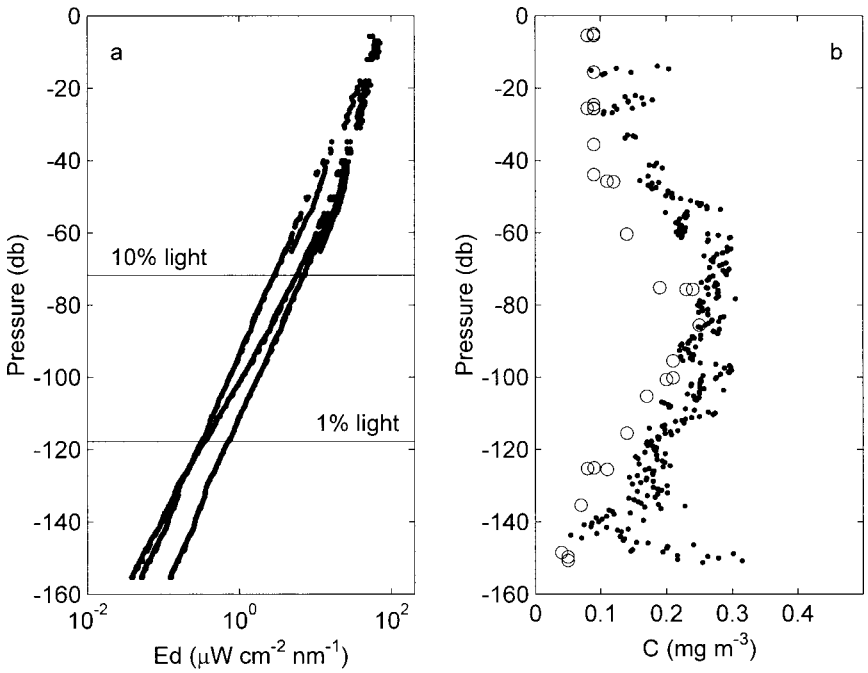

FIG. 6. As for Fig. 5, but irradiance measurements at 412, 443, and 511 nm were used instead.

rometric chlorophyll-*a* measurements in this region is approximately 2%–9% (Santiago-Mandujano et al. 1999). The remaining differences between the estimated and measured values for C may be a result of the use of an incorrect mean cosine, spatial and temporal variations between the datasets, and the vertical displacement of isopycnals (Letelier et al. 1993); the PRR and fluorometric measurements were made on different casts. This analysis was repeated for numerous stations and cruises in the same region, yielding similar results.

At the second location, off the Oregon coast (44°37.75′N, 124°18.82′W), optical profiles at wavebands including 412, 443, and 555 nm were made using a Sea-Viewing Wide Field-of-View Sensor (SeaWiFS) profiling multichannel radiometer (SPMR; Satlantic, Inc.) (Fig. 7a). Measurements were not made at 511 nm. The hysteresis and repeatability of the pressure sensor (Viatran pressure transducer model 222) is 0.1% of full scale (370 m), that is, 37 cm, as is the sensor linearity. Chlorophyll-*a* concentrations measured using the fluorometric method (Fig. 7b) were significantly higher in these coastal waters (up to 7 mg m^{-3}) than those measured at the Hawaiian station. The chlorophyll-*a* concentration was estimated from the SPMR measurements using measurements at 412, 443, and 555 nm, and a mean cosine of 0.8. In this case, a binning interval of 2 m every 0.1 m was sufficient. Comparisons of the estimated C with the extracted chlorophyll measurements show good agreement, both in magnitude and in vertical structure (Fig. 7b). Comparison of the vertical structure of the estimated C with a profile of in situ fluorescence shows excellent agreement except below about 30 m. The outliers in the estimated values at depth are likely caused by the increasing contribution from errors in the irradiance measurements as the magnitude of irradiance decreases (see section 3c).

The third location studied was in the Gulf of California (26.96°N, 110.94°W). The optical profiler was the same as that used off the Oregon coast. Since errors at 555 nm introduced by irradiance measurement noise are non-negligible at depth, results are shown for only the upper 70 m of the 250-m cast. The chlorophyll-*a* concentration was estimated from the SPMR measurements using measurements at 412, 443, and 555 nm, and a mean cosine of 0.8. The measurements were averaged over 1-m bins before being used in the model. The model was used to calculate C and a_y (440) every 1 m with a 5-m depth difference between measurements. In situ chlorophyll-*a* concentrations were estimated from absorption measurements made at the same location using a WET Labs, Inc. ac-9. These chlorophyll values were calculated using the relationship $C = [a_p(676) - a_p(650)]/0.017$, where $a_p(\lambda)$ is the particulate absorption coefficient and 0.017 [m^2/(mg chl)] is the assumed chlorophyll-specific absorption value for phytoplankton at 676 nm (Bricaud and Stramski 1990). Comparisons of C estimated from SPMR measurements with the C calculated from ac-9 data show good agreement, both in magnitude and in vertical structure (Fig. 8a). The difference in the vertical position of the chlorophyll maximum may be a result of internal wave ac-

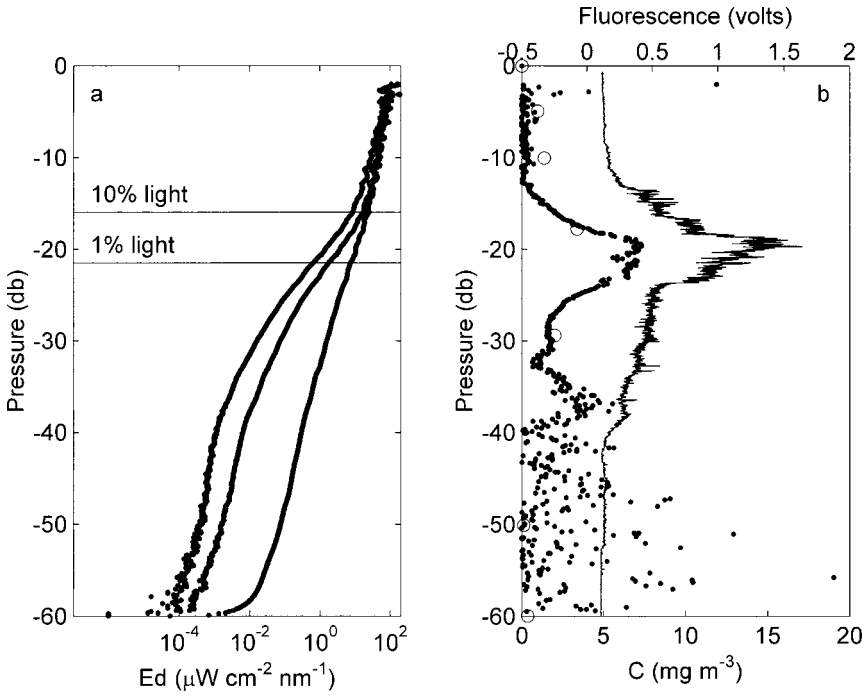

FIG. 7. Downwelling irradiance profiles and chlorophyll-*a* concentration estimated from irradiance profiler measurements off Oregon on 8 Sep 1997 compared with extracted chlorophyll-*a* measurements and in situ fluorometer measurements. (a) Measured downwelling irradiance at 412, 443, and 555 nm (from left to right). (b) Estimated chlorophyll-*a* concentration using the model (for 2000 UTC, filled circles) compared with the measured chlorophyll-*a* concentration (at 2105 UTC, open circles) and measured fluorescence (at 1922 UTC, line). The depths of the 10% and 1% light levels [calculated from $E_d(443)$] are indicated in (a). A mean cosine of 0.8 was used. Bins of 2 m every 0.1 m were used in the model.

tion between the times of the two measurements, which were made 25 min apart.

The same dataset was used to test the model estimates for $a_y(440)$. The modeled and measured values show excellent quantitative and reasonable qualitative agreement (Fig. 8b). Note that the same features are observed in both profiles of $a_y(440)$, although the features are more pronounced in the modeled values.

5. Other applications

This method can also be applied to a number of other deployment methods. To use this method with data from a single instrument, the depth of the instrument must fluctuate. Examples of possible applications include bottom-tethered moorings, towed instruments, autonomous underwater vehicles, and variable-depth moorings or drifters. Alternatively, this method can also be applied to systems with a pair of instruments at different depths. In this case, the instrument depths can be either constant or varying with time. An example would be moorings with two instruments attached to the mooring line.

To apply this method to long-term deployments, such as moorings, care must be taken to choose a time interval between measurements that (i) provides adequate vertical distance between the two measurements (in the case of a single instrument), and (ii) allows minimal variations in the spectral shape of the downwelling light field at the sea surface (e.g., at least two measurements per hour). For these deployments, since the range of depths measured will typically be small (e.g., of the order of 1 m for bottom-tethered moorings), it is crucial to use pressure sensors of high precision to obtain accurate estimates of C.

Note that when using a single instrument whose depth varies, the estimates of C from this method describes the water mass near the measurement depth only. This differs from utilizing two sensors at different depths, which estimate the average chlorophyll-*a* concentration between the two sensors.

6. Conclusions

Chlorophyll-*a* concentration and $a_y(440)$ can be estimated accurately from downwelling irradiance measurements made at varying depths with a single irradiance sensor, provided that (i) the optical contribution from detritus is negligible, (ii) the mean cosine used in the model is accurate, (iii) the pressure sensor measurements are precise, (iv) deployment artifacts are minimized, and (v) the irradiance measurement errors are accounted for by making deployments at appropriate depths. If all of

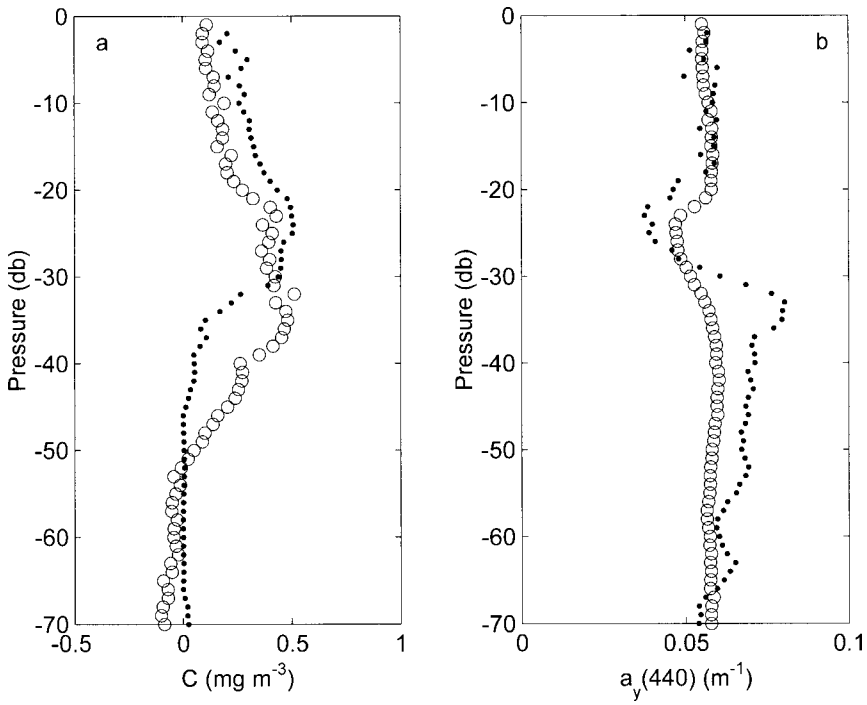

FIG. 8. Chlorophyll-*a* concentration and $a_y(440)$ estimated from irradiance profiler measurements compared with estimates from ac-9 measurements. These measurements were made in the Gulf of California on 25 Apr 1999. (a) Estimated chlorophyll-*a* concentration using the model (at 1932 UTC, filled circles) compared with chlorophyll-*a* concentration estimated from ac-9 measurements (at 1957 UTC, open circles). (b) Estimated $a_y(440)$ using the model (at 1932 UTC, filled circles) compared with $a_y(440)$ from ac-9 measurements (at 1957 UTC, open circles). During the measurements, the sky was clear with some high haze, and the sea was choppy with a 1-m swell. The wind speed was 6 m s^{-1}. A mean cosine of 0.8 was assumed. Data were first averaged over 1-m intervals. Data 5 m apart at 1 m intervals were used in the model.

these conditions are met, this method makes it possible to retrieve information about the biological structure of the water column using just one irradiance sensor. Knowledge of the incident irradiance at the sea surface is not necessary. This allows the deployment of instruments in a more cost-effective manner.

Acknowledgments. We are grateful to Terry Houlihan, Lance Fujieki, and Dave Karl for providing us with PRR measurements and chlorophyll-*a* data, as part of the Hawaiian Ocean Time-Series (HOT) program. We are also grateful to Andrew Barnard for his help with the Oregon SPMR and chlorophyll-*a* data, and Tim Cowles and Russ Desiderio for providing the Oregon fluorometer data. Thanks also to Robert Evans, Katja Fennel, and an anonymous reviewer for their helpful comments on this manuscript. Financial support for this study was provided by NSF (9530507-OPP) and NASA (NAS5-31360).

APPENDIX

Model Derivation

From Eqs. (3), (5), and (6), δK_{ji} can be expressed as a function of C and $a_y(440)$:

$$\delta K_{ji} = [A(\lambda_i, \lambda_j) + B(\lambda_i, \lambda_j)C^{0.65} + D(\lambda_i, \lambda_j)a_y(440)]/\mu_d, \quad \text{(A1)}$$

where

$$A(\lambda_i, \lambda_j) = a_w(\lambda_j) - a_w(\lambda_i),$$

$$B(\lambda_i, \lambda_j) = 0.06[a^*_{\text{ph}}(\lambda_j) - a^*_{\text{ph}}(\lambda_i)], \quad \text{and}$$

$$D(\lambda_i, \lambda_j) = \exp[-0.014(\lambda_j - 440)] - \exp[-0.014(\lambda_i - 440)].$$

The values for the coefficients used in this study are listed in Tables 2 and 3.

Eq. (A1) can be solved algebraically for C and $a_y(440)$ by rewriting it as two simultaneous equations:

$$\delta K_1 = [A_1 + B_1C^{0.65} + D_1a_y(440)]/\mu_d, \quad \text{and} \quad \text{(A2)}$$

$$\delta K_2 = [A_2 + B_2C^{0.65} + D_2a_y(440)]/\mu_d, \quad \text{(A3)}$$

where the subscripts 1 and 2 denote different wavelength pairs [e.g., (412, 443) and (443, 511)]. The pa-

rameter C can then be found by calculating (A2) + γ(A3), where $\gamma = -D_1/D_2$:

$$\delta K_1 + \gamma\delta K_2 = [A_1 + \gamma A_2 + (B_1 + \gamma B_2)C^{0.65}]/\mu_d. \quad \text{(A4)}$$

Rearranging yields

$$C = \{[(\delta K_1 + \gamma\delta K_2)\mu_d - A_1 - \gamma A_2] \div (B_1 + \gamma B_2)\}^{1/0.65}. \quad \text{(A5)}$$

The parameter $a_y(440)$ can then be calculated from (A2):

$$a_y(440) = (\delta K_1\mu_d - A_1 - B_1C^{0.65})/D_1. \quad \text{(A6)}$$

REFERENCES

Bartlett, J. S., M. R. Abbott, R. M. Letelier, and J. G. Richman, 1998a: Chlorophyll concentration estimated from irradiance measurements at fluctuating depths. *Ocean Optics XIV Conf. Papers,* Kailua-Kona, HI, ORN and NASA, CD-ROM.

——, A. M. Ciotti, R. F. Davis, and J. J. Cullen, 1998b: The spectral effects of clouds on solar irradiance. *J. Geophys. Res.,* **103,** 31 017–31 031.

Bricaud, A., and D. Stramski, 1990: Spectral absorption coefficients of living phytoplankton and nonalgal biogenous matter: A comparison between the Peru upwelling area and the Sargasso Sea. *Limnol. Oceanogr.,* **35,** 562–582.

——, A. Morel, and L. Prieur, 1981: Absorption by dissolved organic matter of the sea (yellow substance) in the UV and visible domains. *Limnol. Oceanogr.,* **26,** 43–53.

——, M. Babin, K. Allali, and H. Claustre, 1998: Variations of light absorption by suspended particles with chlorophyll *a* concentration in oceanic (case 1) waters: Analysis and implications for bio-optical models. *J. Geophys. Res.,* **103,** 31 033–31 044.

Carder, K. L., S. K. Hawes, K. A. Baker, R. C. Smith, R. G. Steward, and B. G. Mitchell, 1991: Reflectance model for quantifying chlorophyll *a* in the presence of productivity degradation products. *J. Geophys. Res.,* **96,** 20 599–20 611.

Clarke, G. L., G. C. Ewing, and C. J. Lorenzen, 1970: Spectra of backscattered light from the sea obtained from aircraft as a measure of chlorophyll concentration. *Science,* **167,** 1119–1121.

Gordon, H. R., and A. Y. Morel, 1983: *Remote Assessment of Ocean Color for Interpretation of Satellite Visible Imagery: A Review.* Lecture Notes on Coastal and Estuarine Studies, Vol. 4, Springer-Verlag, 114 pp.

Hoepffner, N., and S. Sathyendranath, 1993: Determination of the major groups of phytoplankton pigments from the absorption spectra of total particulate matter. *J. Geophys. Res.,* **98,** 22 789–22 803.

Kirk, J. T. O., 1994: *Light and Photosynthesis in Aquatic Ecosystems.* 2d ed., Cambridge University Press, 509 pp.

Letelier, R. M., R. R. Bidigare, D. V. Hebel, M. Ondrusek, C. D. Winn, and D. M. Karl, 1993: Temporal variability of phytoplankton community structure based on pigment analysis. *Limnol. Oceanogr.,* **38,** 1420–1437.

——, J. E. Dore, C. D. Winn, and D. M. Karl, 1996: Seasonal and interannual variations in photosynthetic carbon assimilation at Station ALOHA. *Deep-Sea Res.,* **43,** 467–490.

Morel, A., 1974: Optical properties of pure water and pure sea water. *Optical Aspects of Oceanography,* N. G. Jerlov and E. S. Nielsen, Eds., Academic Press, 1–24.

——, 1988: Optical modeling of the upper ocean in relation to its biogenous matter content (case I waters). *J. Geophys. Res.,* **93,** 10 749–10 768.

——, 1991: Light and marine photosynthesis: A spectral model with geochemical and climatological implications. *Progress in Oceanography,* Vol. 26, Pergamon, 263–306.

Pope, R. M., and E. S. Fry, 1997: Absorption spectrum (380–700 nm) of pure water. II. Integrating cavity measurements. *Appl. Opt.,* **36,** 8710–8723.

Prieur, L., and S. Sathyendranath, 1981: An optical classification of coastal and oceanic waters based on the specific spectral absorption curves of phytoplankton pigments, dissolved organic matter, and other particulate materials. *Limnol. Oceanogr.,* **26,** 671–689.

Santiago-Mandujano, F., and Coauthors, 1999: Hawaii ocean time-series data report 10: 1998. SOEST Tech. Rep. 99-05, 249 pp.

Sathyendranath, S., and T. Platt, 1988: The spectral irradiance field at the surface and in the interior of the ocean: A model for applications in oceanography and remote sensing. *J. Geophys. Res.,* **93,** 9270–9280.

——, L. Prieur, and A. Morel, 1989: A three-component model of ocean colour and its application to remote sensing of phytoplankton pigments in coastal waters. *Int. J. Remote Sens.,* **10,** 1373–1394.

Siegel, D. A., and T. D. Dickey, 1988: Characterization of downwelling spectral irradiance fluctuations. *SPIE, Ocean Opt. IX,* **925,** 67–74.

Smith, R. C., K. J. Waters, and K. S. Baker, 1991: Optical variability and pigment biomass in the Sargasso Sea as determined using deep-sea optical mooring data. *J. Geophys. Res.,* **96,** 8665–8686.

Strickland, J. D. H., and T. R. Parsons, 1972: A practical handbook of seawater analysis. Bulletin 167, Fisheries Research Board of Canada, 310 pp.

Ulloa, O., S. Sathyendranath, and T. Platt, 1994: Effect of the particle-size distribution on the backscattering ratio in seawater. *Appl. Opt.,* **33,** 7070–7077.

Waters, K. J., 1989: Pigment biomass in the Sargasso Sea during Biowatt 1987 as determined using deep sea mooring data. M. A. thesis, Dept. of Geography, University of California, Santa Barbara, 136 pp.